Inorganic Chemistry

Article

pubs.acs.org/IC

$[(C_2H_5)_4N][U_2O_4(HCOO)_5]$, an Ammonium Uranyl Formate Framework Showing Para- to Ferro-Electric Transition: Synthesis, Structures, and Properties

Qianqian Zhu, Ran Shang, Sa Chen, Chunli Liu,* Zheming Wang,* and Song Gao*

Beijing National Laboratory for Molecular Sciences, Fundamental Science Laboratory on Radiochemistry & Radiation Chemistry, State Key Laboratory of Rare Earth Materials Chemistry and Applications, College of Chemistry and Molecular Engineering, Peking University, Beijing 100871, China

Supporting Information

ABSTRACT: We report an ammonium uranyl formate framework of formula $[(C_2H_5)_4N][U_2O_4(HCOO)_5]$, prepared by using components of tetraethylammonium, uranyl, and formate. The compound possesses a layered structure of anionic uranyl–formate wavy sheets and intercalated $(C_2H_5)_4N^+$ cations. The sheet consists of pentagonal bipyramidal uranyl cations connected by equatorial *anti–anti* and *anti–syn* $HCOO^-$ bridges, and it has a topology of $3^3{\cdot}4^3{\cdot}5^4$ made of edge-sharing square and triangle grids. The high-temperature (HT) phase belongs to the chiral but nonpolar tetragonal space group $P\bar{4}2_1m$. In the structure, one $HCOO^-$ is 2-fold disordered, showing a flip motion between the two *anti–syn* orientations. On cooling, this flip motion slowed and finally froze, leading to a phase transition at ~200 K. The low-temperature (LT) structure is monoclinic and polar in space group $P2_1$; the cations shift, and the layers slide. Especially, the concerted and net shifts of the ammonium cations toward the $-b$ direction, with respect to the anionic sheets, result in an estimated spontaneous polarization of 0.86 μC cm^{-2} in LT. The phase transition is thus para- to ferroelectric, in Aizu notation $\bar{4}2mF2$, accompanied by significant, anisotropic dielectric anomalies, with a quite significant thermal hysteresis. Variable-temperature luminescent spectroscopy and differential scanning calorimetry confirmed the transition and provided further information. The structure–property relationship is established.

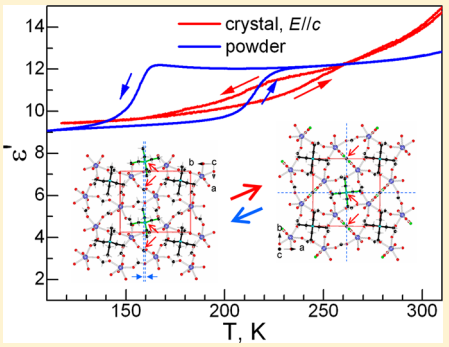

INTRODUCTION

In the last two decades metal–organic frameworks (MOFs) have been extensively studied due to their very wide spectrum of properties, functionalities, and possible applications.[1,2] In this very active research area, there is an emerging realization that MOFs can display diversity in their physical properties and critical phenomena or phase transitions, probably as rich as that in traditional materials.[3] Recently, dielectric (DE) and ferro-/antiferro-electricities (FE/AFE) of MOFs, closely relevant to their structural or phase transitions, have aroused quite a lot of interest, both fundamental and practical.[4] Clearly, MOFs are promising for such materials because the requests for DE/FE/AFE properties could be satisfied if the related functional building blocks (hydrogen-bonding (HB) donors and acceptors, polar solvents, etc.) or structural features (space or freedom for order–disorder transitions of the components, for example) are incorporated.[1d,2e,4] In this context, it has been proven that the ammonium metal formate frameworks (AMFFs), being a class of MOFs, exhibit unique DE/FE/AFE properties, which could coexist or combine with other properties such as magnetism.[5−14] This is because such a combination of ammonium, metal ion, and formate is beneficial for the formation of different frameworks, required HB systems, and phase transitions, triggered by the order–disorder alteration of the components (mainly the ammonium), for DE/FE/AFE, and the effective magnetic coupling between magnetic sites through the short formate bridges.[5] Many AMFFs, in the formula of $[AH][TM(HCOO)_3]$,[6−11] where TM = 3*d* transition metal or Mg and AH = monoammonium from the small NH_4^+ to large ones such as guanidinium and imidazolium, displayed FE/AFE and their coexistence or synergism with magnetism, large dielectric anomalies, relaxation behaviors, and so on. Temperature/pressure-induced structural transitions have been observed in several lanthanide AMFF systems.[12] Unusual mechanical properties such as negative thermal expansion or negative linear compressibility have been documented for AMFFs.[6,7] The research has also been extended from mono- to polyammoniums,[5,12,13] which possess more freedom of molecular motion. For example, the niccolite of $[dmenH_2][TM(HCOO)_3]_2$ ($dmenH_2^{2+}$ = diprotonated *N,N′*-dimethylethylenediamine)[13] and a pillared layer lanthanide (Ln) AMFF, $[tmenH_2][Er(HCOO)_4]_2$ ($tmenH_2$ = diprotonated *N,N,N′,N′*-tetramethylethylenediamine)[12] display phase transitions and the related structural alternations resulting from the freeze of rotational motion of the diammoniums and/or flip motion of some formato ligands.

Received: June 8, 2014
Published: July 29, 2014

   dx.doi.org/10.1021/ic501336x | *Inorg. Chem.* 2014, 53, 8708–8716

Table 1. Crystallographic Data for 1 at 290, 250, and 180 K

formula		$C_{13}H_{25}N_1O_{14}U_2$	
fw		895.40	
T, K	290	250	180
crystal system	tetragonal	tetragonal	monoclinic
space group	$P\bar{4}2_1m$	$P\bar{4}2_1m$	$P2_1$
a, Å	12.3383(2)	12.3262(2)	11.5792(11)
b, Å	12.3383(2)	12.3262(2)	12.8431(9)
c, Å	8.1137(5)	8.0856(5)	8.6056(7)
α, deg	90	90	90
β, deg	90	90	107.657(9)
γ, deg	90	90	90
V, Å^3	1235.18(8)	1228.49(8)	1219.47(17)
Z	2	2	2
D_c, g/cm^3	2.408	2.421	2.439
$F(000)$	812	812	812
μ (Mo Kα), mm^{-1}	13.154	13.226	13.324
crystal size, mm^3	0.26 × 0.24 × 0.24	0.26 × 0.24 × 0.24	0.33 × 0.23 × 0.17
T_{min}, T_{max}	0.087, 0.222	0.086, 0.220	0.091, 0.367
θ_{min}, θ_{max}, deg	3.43, 28.26	3.44, 28.28	3.52, 25.02
no. total reflns.	20 839	20 709	15 494
no. uniq. reflns. (R_{int})	1633 (0.0851)	1623 (0.0840)	4102 (0.1224)
no. obs. [$I \geq 2\sigma(I)$]	1450	1462	3658
no. params	85	85	131
R_1,[a] wR_2[b] [$I \geq 2\sigma(I)$]	0.0378, 0.0815	0.0342, 0.0772	0.0744, 0.1687
R_1,[a] wR_2[b] (all data)	0.0461, 0.0872	0.0417, 0.0824	0.0838, 0.1768
GOF	1.056	1.081	1.034
Flack parameter	0.07(3)	0.06(3)	0.02(3)
$\Delta\rho$, e/Å^3[c]	1.821, −2.647	1.762, −2.594	4.892, −2.284
max. and mean Δ/σ[d]	0.000, 0.000	0.001, 0.000	0.000, 0.000

[a] $R_1 = \sum||F_o| - |F_c||/\sum|F_o|$. [b] $wR_2 = [\sum w(F_o^2 - F_c^2)^2]/\sum w(F_o^2)^2]^{1/2}$. [c] Maximum and minimum residual electron density. [d] Maximum and mean shift/sigma.

By far the most investigated AMFFs are those of TM and Ln.[5−14] It is natural to extend the research to the actinides (Ac), and we recently started a systematic research. The uranyl cation UO_2^{2+} is the most popular one of the Ac ions. It favors bipyramidal coordination and thus is a unique and useful building block for constructing MOFs. There are increased interests in such compounds recently,[15] in parallel with the studies of TM and Ln systems, due to the structure richness and the possible applications. However, a literature survey revealed that the known uranyl AMFFs are very limited,[16] indicating that they were ignored by researchers, a very similar case to the study of TM/Ln AMFFs 10 years ago.[5,8a,9e] The employed ammonium cations include NH_4^+,[16a] $(C_2H_5)_3NH^+$,[16b] and $[dabcoH_2]^{2+}$ (dabco = 1,4-diazabicyclo-[2.2.2]-octane),[16c] and the uranyl−formate chains and sheets were formed. The uranyl−AMFF systems should be of interest for phase transitions and DE/FE/AFE properties, similar to the TM/Ln AMFFs[5] and other ammonium systems.[4a−d] In this work, we report $[(C_2H_5)_4N][U_2O_4(HCOO)_5]$ (**1**) characterized by thermal analyses, single-crystal X-ray diffraction (SXRD), powder X-ray diffraction (PXRD), variable-temperature (VT) spectroscopy, and dielectric measurement. The material possesses a layered structure, composed of anionic uranyl−formate sheets with tetraethylammonium $(C_2H_5)_4N^+$ cations intercalated. It underwent a para-electric (PE) to FE transition at ∼200 K, with the lattice symmetry changed from high-temperature (HT) tetragonal $P\bar{4}2_1m$ to low-temperature (LT) monoclinic $P2_1$, caused by the freezing of the flip motion of a disordered formate ligand and the related shift of the cation with respect to the anionic sheets. VT luminescent spectroscopy, differential scanning calorimetry (DSC), and dielectric studies characterized the phase transition, and the structure−property relationship was established.

EXPERIMENTAL SECTION

Synthesis. All starting chemicals were commercial reagents of analytical grade and were used without further purification. AMFF **1** was synthesized by a mild solution method. A methanol solution of 25% tetraethylammonium hydroxide (118 mg) and an ethanol solution (2.0 mL) of 4.0 M formic acid were mixed in a glass vial. An ethanol solution (200 μL) of 0.50 M $UO_2(NO_3)\cdot 6H_2O$ was gently added, and the vial was sealed and left undisturbed. Block or plate yellow crystals of X-ray quality were obtained after 2 d. They showed easy cleavage along large face. The crystals were collected, washed with ethanol, and dried in air. The yield was 56% based on $UO_2(NO_3)\cdot 6H_2O$. Anal. Calcd for $C_{13}H_{25}NO_{14}U_2$: C 17.44, H 2.81, N 1.56%; found: C 17.44, H 2.75, N 1.62%. ***Caution!*** *Because uranium is a radioactive and chemically toxic element, uranium-containing samples must be handled with suitable care and protection.*

X-ray Crystallography and Physical Measurements. The SXRD intensity data for **1** at 180, 250, and 290 K were collected on an Agilent Technology SuperNova Dual Atlas CCD diffractometer, equipped with monochromated Mo Kα radiation (λ = 0.710 73 Å) and a temperature-control system.[17] The structures were solved by direct methods and refined by full-matrix least-squares on F^2 using SHELX program.[18] The H atoms were added according to the ideal geometry. Because of the cracking of the crystal, the quality of the intensity data at 180 K is not as good as usual, and the anisotropic refinement resulted in nonpositive thermal parameters for many C/N/O atoms. They were thus refined isotropically. Attempts to improve the data quality were proven unsuccessful. Crystallographic data are listed in

dx.doi.org/10.1021/ic501336x | Inorg. Chem. 2014, 53, 8708−8716

Table 2. Selected Bond Distances (Å) and Angles (deg) and C−H···O Hydrogen Bonds (Å and deg) of 1 at the Three Temperatures

T, K	290	250	180
U−O_{ax}	1.729(14), 1.774(11)	1.736(12), 1.768(10)	1.731(16)−1.800(16)
U−O_{eq}	2.34(3)−2.43(2)	2.33(2)−2.459(19)	2.347(19)−2.450(18)
C−O	1.20(3)−1.232(12)	1.196(17)−1.240(10)	1.204(17)−1.28(3)
C−C	1.52(2)	1.524(19)	1.46(4)−1.57(4)
C−N	1.507(12)	1.502(10)	1.47(3)−1.54(4)
O_{ax}−U−O_{ax}	179.0(6)	179.0(5)	178.0(9), 179.5(8)
O_{ax}−U−O_{eq}	75.5(10)−105.5(9)	76.3(8)−104.7(8)	85.1(6)−95.3(7)
O_{eq}−U−O_{eq}	71.0(3)−145.6(4)	70.9(3)−145.8(4)	70.2(6)−146.5(6)
U−O−C	129.7(7)−149(2)	129.4(6)−149.4(19)	126.9(16)−141.7(17)
O−C−O	126(1), 126(2)	126(1), 127(2)	120(3)−130(2)
N−C−C	116.2(9)	116.0(8)	114(2)−117(2)
C−N−C	105.9(1), 111.3(5)	104.6(9), 111.9(5)	105.4(2)−114(2)
C−H···O	>3.5, see text	>3.5, see text	3.37−3.45, 146.8−172.1

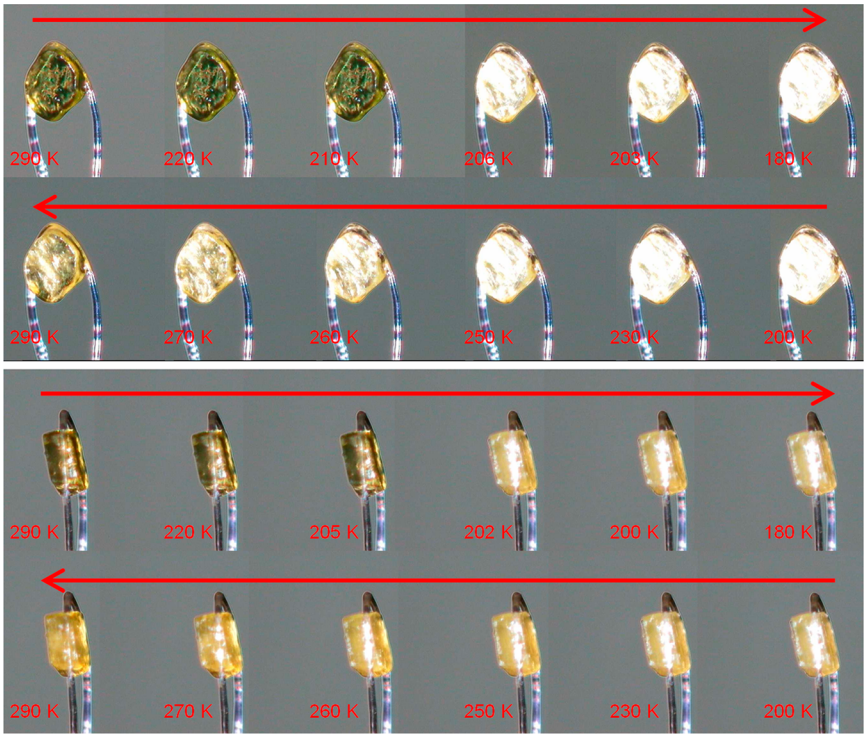

Figure 1. Variable-temperature photos of two crystals under the microscope of the CCD diffractometer on cooling-warming cycle. For the top one, the face (001) points toward. For the bottom one, the face (001) points to the left.

Table 1, and selected molecular geometries are presented in Table 2. VT photos for two crystals were collected under the microscope of the same diffactometer. PXRD data for the as-prepared and pressed tablet samples, and the residue sample of pyrolysis, were collected at room temperature (RT) on a Rigaku Dmax 2000 diffractometer with Cu Kα radiation in a flat plate geometry.

Element analysis of C/H/N was performed on an Elementar Vario MICRO CUBE analyzer. Thermal analysis was performed from RT to 1000 °C on a TA SDT Q600 simultaneous DSC-TGA (TGA = thermogravimetric analysis) instrument at the rate of 5 °C min^{-1} in air flow. The DSC measurement was performed on a TA Q2000 DSC analyzer at the rate of 5 °C min^{-1} in N_2 flow and cycled twice. Spectroscopic studies were performed against the pure solid samples of the compound. IR spectrum was recorded on NICOLET iN10 MX spectrometer in the range from 4000 to 600 cm^{-1}. Raman spectrum was collected on a HORIBA Jobin Yvon LabRAM ARAMIS micro-Raman spectrometer with an excitation wavelength of 633 nm. UV−vis reflectance spectrum was recorded on a SHIMADZU UV−vis 2450 spectrophotometer with an integrated sphere attachment in the range of 300−600 nm, by using a $BaSO_4$ background. Fluorescence studies were carried on an Edingburgh FLS920 fluorescence spectrometer equipped with an LT system.

The temperature-dependent alternative current (ac) dielectric permittivity measurements were carried out on a TH2828 Precision LCR meter and a homemade temperature-control system. For the capacitor made by crystal, a plate-shaped crystal was used, with the two opposite large faces painted with silver paste, and gold wires as the electrodes. The faces are (001) as shown in Figure S1 of the Supporting Information. For the powder capacitor, the samples were ground and pressed into a tablet under ca. 2 GPa, and the capacitor was made using a tablet piece. These capacitors were kept vacuum-dried over silica gel for more than 10 d and were then finally coated by AB glue before making dielectric measurements. The area and thickness of the capacitors were measured under an optical microscope with a Phenix CCD eye and the software. Unfortunately, the crystals were not large and thick enough for preparing crystal capacitors with, for example, faces like (100) or (010).

dx.doi.org/10.1021/ic501336x | Inorg. Chem. 2014, 53, 8708−8716

RESULTS AND DISCUSSION

Synthesis, PXRD, VT Photos of Crystals, Thermal Property, and Phase Transition. The previous studies on the AMFFs[5−8,10,12−14] have demonstrated that such materials can be prepared through convenient solution chemical methods at ambient temperature, by employing suitable metal salts, ammoniums, and formate. We have expanded our research to uranyl, and indeed, these synthetic methods have worked well in preparing the related uranyl AMFFs.[19] In the present study, the compound was successfully obtained with satisfactory yield, confirming this point. The bulk-phase purity was verified by PXRD (Figure S2 in Supporting Information). The pressed tablet sample remained the phase unchanged, but the diffraction ability seemingly became weaker and the signal noisy, probably due to the formation of a large number of defects in tablet preparation, grinding, and pressing.

A phase transition was first observed by finding the crack of a single crystal of **1** at 180 K. Two crystals were used to confirm this initial observation and to find the transition temperature (T_C). They were mounted on the diffaractometer at RT, then cooled, and the VT photos were taken under the diffractometer's microscope (Figure 1). One crystal had its large face (001), the cleavage face (Figure S1 in Supporting Information), toward forward, and the other had the face toward left roughly. The yellow crystals remained unchanged and transparent until ca. 200 K when they suddenly became opaque and finely cracked. Subsequently, the samples were warmed from 180 to 290 K. The crystal samples become somewhat more transparent at ∼260 K. When returning to 290 K, the samples became semitransparent. This confirmed the previous observation about the phase transition, and the T_C was about 200 K on cooling, but ca. 250 K on warming, indicating a 50 K thermal hysteresis behavior for the phase transition.

The DSC traces (two cycles, Figure 2) of **1** showed reversible, broad exo/endothermic peaks around 200/250 K upon cooling/heating, though the exothermic peaks were not well-defined because they were close to the LT limit (−80 °C) of the DSC instrument. The temperatures for the occurrence of the phase transition are agreeable to the above observation on VT crystal photos. From the endothermic peak on warming, the ΔH value of the phase transition was estimated to be 2.1 kJ mol^{-1}, and the ΔS value ($\Delta S = \Delta H/T_C$;[20] T_C = 250 K was used) was estimated as 8.2 J mol^{-1} K^{-1}. By applying the Boltzmann equation $\Delta S = R\ln(N)$, where R is the gas constant and N is the ratio of the numbers of distinguishable states of different phases, we obtained N = 2.7, and this is related to the structure alternation during phase transition (see subsequent discussion).

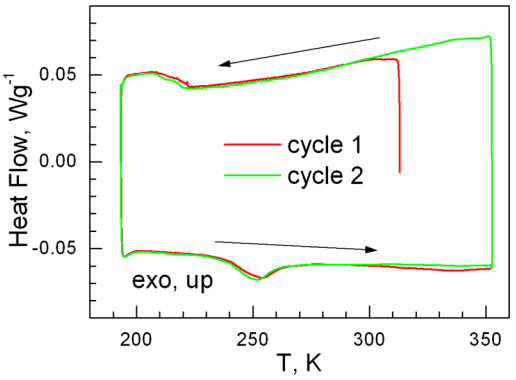

Figure 2. DSC trace for **1**, two cycles.

The combined TGA and DSC traces are shown in Figure S3a in Supporting Information. The compound was thermally stable up to 200 °C. Above 250 °C, the significant weight loss occurred, the pyrolysis seemingly consists of two steps merged together, and the energy release is about 1.8 × 10^3 kJ mol^{-1}, indicating a strong exothermic process. The residue at 350 °C was 63.7%, agreeable with the calculated value of 63.9% for the intermediate UO_3. A weight loss of 1.5% further occurred from 350 to 700 °C, forming the final residue of U_3O_8, confirmed by the PXRD pattern of the residue (Figure S3b in Supporting Information), and the final residue at 1000 °C is 62.1% versus calculated 62.7% based on U_3O_8.[21]

Crystal Structures. The HT phase belongs to tetragonal space group $P\bar{4}2_1m$, chiral but nonpolar in the point group D_{2d} (Table 1). The appearance of the chirality in crystal **1** represents a case that incorporating multiple acentric centers within the lattice by using simple, acentric but achiral building blocks could provide good chance to obtain chiral crystalline solids.[14] The layered structure consists of anionic uranyl−formate sheets with intercalated $(C_2H_5)_4N^+$ cations (Figures 3 and 4). The unique uranyl cation is 5-fold coordinated in its equatorial plane by five individual $HCOO^-$ bridges, four *anti*−*anti*, and one *anti*−*syn*, connecting to the five neighbor uranyl cations (Figure 3a), to form the wavelike sheet extending in *ab* plane (Figure 3b). One 2-fold disordered $HCOO^-$, with the C

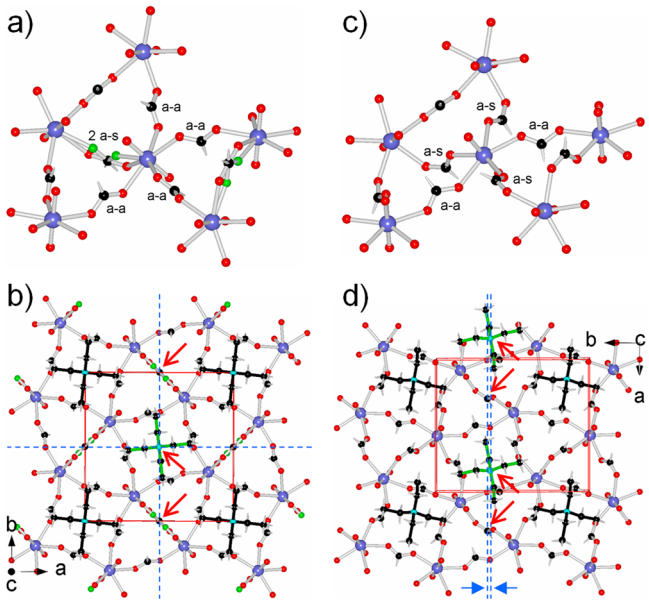

Figure 3. Structure of **1**: (a) and (b) at 290 K, (c) and (d) at 180 K. In (a) and (c) the central uranyl cation is connecting to the five neighbors through five *anti*−*anti* (a-a) or *anti*−*syn* (a-s) formate bridges, noting the changes of the bridging mode of formates from (a) to (c). In (a) and (b) the two orientations of the disorder *anti*−*syn* formate are represented by two green-red O pairs. In (b) and (d), the blue dot lines crossing the C2 atoms, indicated by the red left-down arrows, represent the symmetric planes of the anionic sheets. The N atoms of cations are indicated by the red left-up arrows. In (d) the right blue dot line crosses N atoms, together with the two blue arrows, indicating the small shift of cations with respect to the anionic sheets in −*b* direction; see text. Color scheme: U violet-blue, C black, H white, O red/green, N cyan. In (b) and (d) the middle cations have green C−C/N bonds, but the left and right have black C−C/N bonds.

dx.doi.org/10.1021/ic501336x | *Inorg. Chem.* 2014, 53, 8708−8716

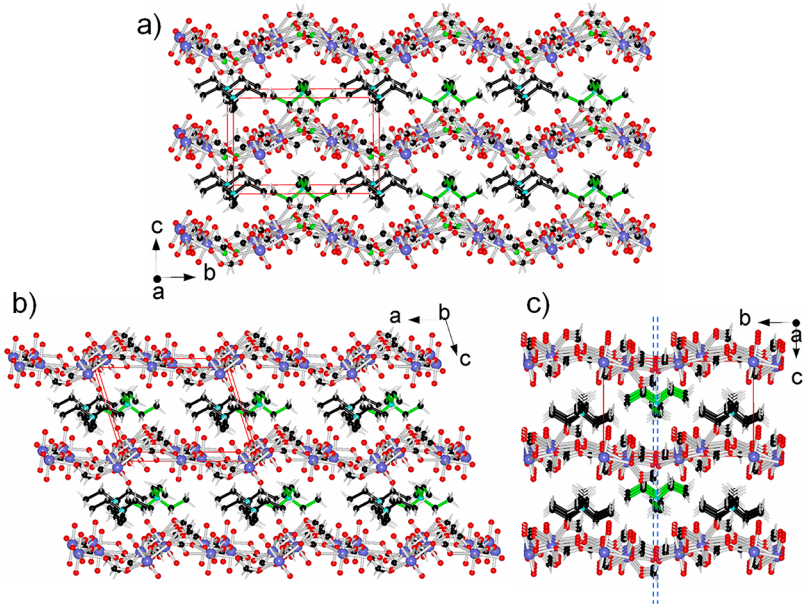

Figure 4. Stacking structure of **1** (a) at 290 K, along *a* axis, and (b) and (c) at 180 K, along *b* and *a* directions, respectively. Color scheme and the meaning of two blue lines are the same as that in Figure 3.

atom (C2:1/2, 0, −*z*) at the Wyckoff *c* site (2.*mm*), showed two *anti*−*syn* orientations, in which the C/H/O atoms are all in the mirror plane extending in *c* direction. The layer has a topology of $3^3{\cdot}4^3{\cdot}5^4$, but could be considered as a (4, 4) one composed of square and rhombic grids alternatively arranged, with *anti*−*anti* $HCOO^-$ edges, and the rhombic one has its short diagonal crossed by the 2-fold disordered *anti*−*syn* $HCOO^-$. The layer thus consists of square and triangle grids sharing their edges, similar to the Ln-formate layer reported in $[tmenH_2][Er(HCOO)_4]_2$.[12] At 290 K, the pentagonal bipyramid UO_7 moiety has the U−O distances of 1.729(14) Å and 1.774(11) Å for the axial U−O_{ax} bonds and from 2.34(3) to 2.43(2) Å for the equatorial U−O_{eq} bonds, and O−U−O angles from 71.0(3) to 179.0(6)° (Table 2). These data are comparable with those of the reported uranyl−formate-based compounds.[16,22] The formate-bridged U···U distances are 5.867 and 6.599 Å for the disordered *anti*−*syn* $HCOO^-$ and *anti*−*anti* ones, respectively. The apical O atoms of linear UO_2^{2+} point up and down aslant since the layer is wavy, equivalently along both *a* and *b* directions, and the 2-fold disordered *anti*−*syn* $HCOO^-$ groups occupy the peaks and troughs (Figure 4a). These anionic layers stack along the *c* direction and overlap one another, and the interlayer regions are occupied by $(C_2H_5)_4N^+$ cations. Viewed down the *c* axis (Figure 3b), the cation, with a completely extending conformation and the central N at $\bar{4}$ (N1:1/2, 1/2, 0; Wyckoff *a* site), just covers the square grids of the layer, compatible to the lattice $\bar{4}$ symmetry. The C···O distances between the C−H groups of the cation and the O of the layer are beyond 3.53 Å; thus, no significant HBs were observed. At 250 K, the structure remained unchanged but shows a slightly smaller lattice and related changes in molecular geometries (Tables 1 and 2).

The material underwent a phase transition at ∼200 K on cooling, and the crystal finely cracked (Figure 1). Fortunately, the structure of the LT phase at 180 K could be obtained on the diffraction data collected on a cracked crystal (Figures 3c,d and 4b,c), and the quality of the LT structure is good enough to reveal the structural alternation during phase transition. The LT phase is chiral and polar, in monoclinic space group $P2_1$ and point group C_2. From HT to LT, only 2_1 remains along a^{HT} direction, and other symmetry elements of the HT phase are lost. In Aizu notation,[23] this is a $\bar{4}2mF2$ ferroelectric transition, indicating that the LT phase is ferroelectric. The relationship between the HT and LT cell settings is $a^{HT} \approx -b^{LT}$, $b^{HT} \approx -a^{LT}$, and $c^{HT} \approx -c^{LT}$ (Figure 3b,d). In the HT setting, taking the data of 250 and 180 K (Table 1), the *a* and *c* axes expanded 0.52 Å, but *b* shrank 0.75 Å, the α^{HT}, that is, β^{LT}, changed from 90° to 107.66°, and the cell volume is ca. 10 $Å^3$ smaller. In the LT structure, the uranyl−formate layer remains with its topology unchanged. Instead, the *anti*−*anti* $HCOO^-$ groups along b^{HT} direction changed to *anti*−*syn*, and those along a^{HT} remained *anti*−*anti* and changed their orientations slightly. The more important observation is that the 2-fold disordered *anti*−*syn* $HCOO^-$ ligands in HT froze and became ordered *anti*−*syn* in LT. Accompanying such changes, half of the ammonium cations, still in an extending conformation, shift in the $-b^{LT}/a^{HT}$ direction, and the other half of the ammonium cations, related by $2_1 \| b$, shift opposite and equally. The uranyl−formate sheets showed related slides one to another in the *a* direction. The expansion of *c* axis is due to such sheet slide, but the interlayer distance changes a little. The layer is still wavy along the *a* direction, while it becomes flat along the *b* direction (Figure 4b,c). The changes are so large that the crystal cracked, and this case is still uncommon for AMFFs.[6a] It is noted that all ammonium cations move slightly along the −*b* direction, with respect to the anionic layers (Figure 3d and Figure 4c). All these resulted in the changes in the cell parameters and lattice symmetry and contributed to the *N* value of 2.7 derived from DSC data, significantly larger than the sole contribution of the disorder−order transition of the formate bridge, which has two discrete states in the HT phase but one in the LT phase, providing *N* = 2. The molecular geometries of the LT structure, that is to say, the U−O distances and O−U−O angles, show slightly more dispersion, and the U···U distances are 5.906−6.244 Å through *anti*−*syn* $HCOO^-$ and 6.733−6.753 Å via *anti*−*anti* ones, respectively. Some shorter C···O contacts of 3.36−3.45 Å between the ammonium cation and the O of the layer are observed, indicating the formation or enhancement of

dx.doi.org/10.1021/ic501336x | *Inorg. Chem.* 2014, 53, 8708−8716

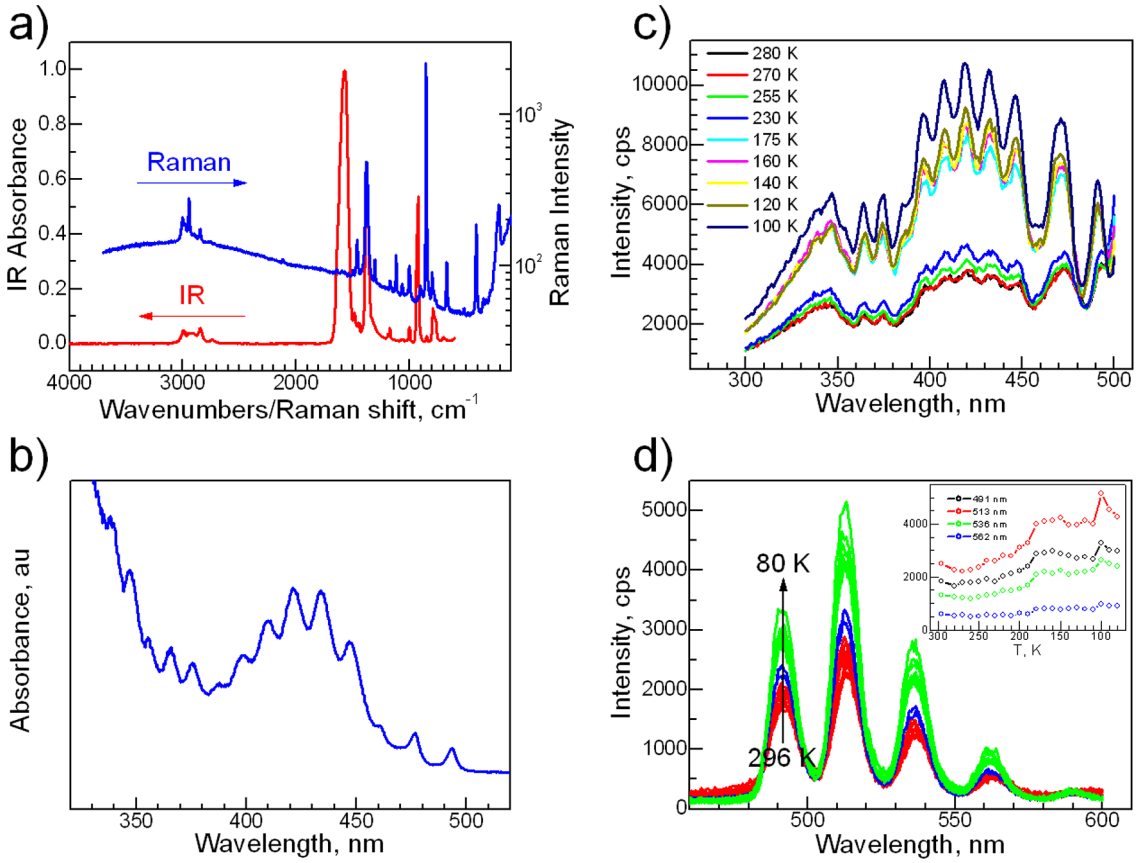

Figure 5. Spectroscopic properties of **1**: (a) IR and Raman spectra, (b) solid UV-vis reflectance spectrum, (c) variable-temperature excitation spectra, and (d) variable-temperature emission spectra and (inset) the four band intensity vs temperature plots.

the weak C−H···O HBs,[24] which might be an important driving force for the phase transition.

The polarization of the LT phase is induced by the slight but concerted shifts of all cations along the $-b$ direction (Figures 3d and 4c). In the structure of the nonpolar HT phase (Figure 3b), from the viewpoint of symmetry, the plane crossing the C atoms of the 2-fold ordered *anti*−*syn* $HCOO^-$, at the middle points of *a*-period and extending in *c*-direction or including the $\bar{4}$ axis, is the symmetric plane of the charge distribution of the anionic layer, and the plane includes the cations. We assume that the plane remains (at least approximately) symmetric for the charge distribution of the anionic part in the structure of LT phase. Now the cations are all off the plane, with the shifts of the central N atoms, 0.325 Å, in $-b$ direction. This could be considered as the separation of the two point charges, negative from the layer and positive from the cations, in the generated dipole.[6,7a,b] Therefore, the polarization of the LT phase at 180 K was calculated as 0.86 μC cm^{-2} by two such dipoles per unit cell, and it points to $-b$ direction. This is rational for AMFFs[6,7a,b,8a] or MOF-based ferroelectrics[4a,b] but merits further confirmation by experimental and theoretical investigation.

Infrared, Raman, UV−vis and Luminescent Spectra. The IR and Raman spectra (Figure 5a and Supporting Information, Table S1) of AMFF **1** showed the bands characterizing the components of ammonium, formate, and uranyl, and the spectra are complementary.[25,26] In the IR spectrum, the presence of the $(C_2H_5)_4N^+$ cation is confirmed by weak broad bands between 2993 and 2739 cm^{-1} assigned to C−H bond stretching vibrations, the related weak or middle bands at 1486, 1455, and 1442 cm^{-1} are assigned to the deformation of the CH_2/CH_3 groups, the bands at 1185 and 1173 cm^{-1} indicate C−N/C stretching, and the band at 1001 cm^{-1} indicates C−H out of deformation. Strong bands at 1573 and 1378 cm^{-1} are antisymmetric (ν_4) and symmetric (ν_5) stretchings of formate, respectively. The difference $\Delta\nu = \nu_4 - \nu_5$ is 195 cm^{-1}, indicating the bidentate or bridging coordination mode[25a] of formate in the structure, as revealed by SXRD. The symmetric deformation of formate appeared at ca. 800 cm^{-1}. All these bands could also be observed in the Raman spectrum though most of them are weak. The three modes[26] of uranyl cation are observed. The asymmetric stretching is IR active but Raman inactive, thus a quite strong band appeared at 925 cm^{-1} in IR but a weak band appeared at 905 cm^{-1} in Raman. Instead, the symmetric stretching (ν_s) is IR inactive but Raman active; thus, it is weak at 848 cm^{-1} in IR and strong at 855 cm^{-1} in Raman. The bending mode δ also appeared at 212 cm^{-1} in the Raman spectrum. According to Bartlett et al.,[27] d(U−O) (in pm) = (10 650)[ν_s (in cm^{-1})]$^{-2/3}$ + 57.5; for the U−O_{ax} bond length of uranyl and the symmetric stretching in Raman, we obtained U−O_{ax} = 1.76 Å in **1**, matching the averaged value of 1.75 Å from SXRD data at 290 K.

The solid UV−vis reflectance spectrum of **1** in the range of 330−520 nm (Figure 5b) consists of 10 bands with peak positions of 347, 356, 366, 376, 388, 398, 410, 421, 434, 447, 460, 477, and 493 nm. Bands in the range from 345 to 420 nm can be assigned to transitions $^1\Sigma_g^+ \rightarrow {}^1\Phi_g$ and $^1\Sigma_g^+ \rightarrow {}^1\Delta_g$, while bands between 420 and 500 nm can be assigned to the transitions of $^1\Sigma_g^+ \rightarrow \Pi_g$ and $^1\Sigma_g^+ \rightarrow {}^1\Delta_g$, based on the

dx.doi.org/10.1021/ic501336x | Inorg. Chem. 2014, 53, 8708−8716

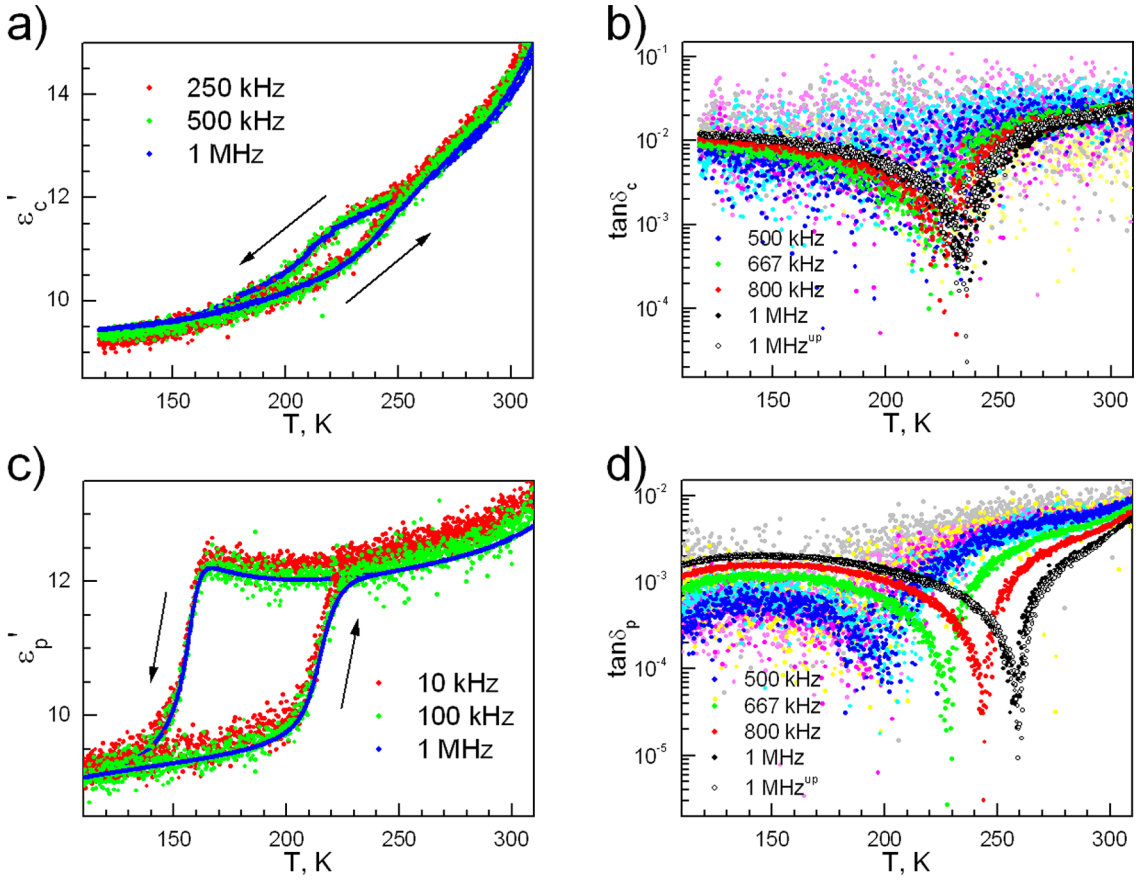

Figure 6. Temperature-dependent traces of the dielectric permittivities for **1**: (a, b) for crystal capacitor with the applied $E\|c$, (c, d) for powder capacitor. In loss data (b, d) only plots for frequencies of 500, 667, 800, and 1000 kHz are labeled because below 500 kHz the signals are noisy.

previous studies.[28] These absorption bands are typical for uranyl ions and show the superimposition of the symmetric stretching vibration of uranyl. The excitation spectra of **1** (Figure 5c), monitored at 514 nm, showed bands almost the same as those in the UV−vis spectra of **1**, indicating the relevance. The bands are more enhanced and better defined below 175 K, and the gap between HT and LT is related to the phase transition. The VT emission spectra (Figure 5d, excited by 330 nm light) from RT to 80 K in 10 K steps all display five bands at 492(m), 513(s), 536(m), 562(w), and 589(vw) nm, typically observed for uranyl compounds.[29] The average spacing of the five bands is 840 cm^{-1}, which is the symmetric stretch of the uranyl ion, agreeing quite well with the observations in IR and Raman spectra. The band intensities were enhanced on cooling, and the temperature-evolution displayed a significant increase between 190 and 180 K (Figure 5d, inset). As the structural study revealed, on cooling, not only are the vibrations of constituent atoms reducing but the more important fact is that the 2-fold disordered *anti*−*syn* $HCOO^-$ ligands in HT became ordered *anti*−*syn* in LT. The structural change due to phase transition reduced the radiationless transition significantly,[30] and thus enhanced the luminescence. Therefore, the VT luminescent spectroscopy could also reveal the phase transition in the present case.

Dielectric Property and the Relevance to Phase Transition. The temperature-dependent complex dielectric permittivity (real component ε' and loss $\tan\delta$) of **1** was investigated for two capacitors, one for a plate crystal with the applied $E\|c$ (ε_c' and $\tan\delta_c$), and the other for powder tablet (ε_p' and $\tan\delta_p$), both on one cooling-warming cycle. For the crystal capacitor (Figure 6a,b), on cooling, the ε_c' value at 1 MHz decreased, first quickly and then slowly, from 14.7 at 310 K to 11.4 at ∼220 K, then the decrease speeded up again at ∼210 K, leading to a shoulder there, and further went down to 9.5 at 116 K. In the succeeding warming, the ε_c' value gradually increased, rose more quickly above 230 K, and above 260 K it nearly superimposed the cooling plot. The temperatures for the observed dielectric anomalies, ∼210/240 K on cooling and warming, respectively, are agreeable to the DSC and VT-photo studies, though the thermal hysteresis of ca. 30 K is somewhat smaller. The $\tan\delta_c$ trace at 1 MHz showed a minimum at ∼235 K. Above 200 kHz the ε_c' response was frequency-independent, but the minima of $\tan\delta_c$ slightly moved to low temperatures for low frequencies (to ca. 210 K for 500 kHz) and showed no hysteresis behavior. Below 200 kHz the dielectric responses were noisy, partially due to the small size of the capacitor. The dielectric data for the powder capacitor showed quite different behavior (Figure 6c,d). On cooling, the ε_p' value of 1 MHz decreased slowly from 12.7 at 310 K to a shallow minimum of 11.0 at ∼210 K, then increased slowly to a maximum of 12.2 at ∼170 K. After that it quickly fell between 160 and 150 K, and finally it reached 9.1 at 110 K. In the subsequent warming, the ε_p' value gradually increased to 9.7 at 200 K, then increased quickly from 210 to 230 K, and above 250 K it coincided with the cooling plot. Compared with the crystal capacitor, the thermal hysteresis of ca. 60 K is more significant, and the temperature for dielectric anomalies seemingly shifted ca. 30 K lower. Above 10 kHz the ε_p' plots were not scattered very much

dx.doi.org/10.1021/ic501336x | *Inorg. Chem.* 2014, 53, 8708−8716

and were not frequency-dependent. The tanδ_p versus T plots above 200 kHz showed frequency-dependent minima, from 260 K at 1 MHz to 170 K at 200 kHz, without thermal hysteresis. This frequency-dependence is more significant than the crystal capacitor. In the LT region the loss plots displayed low, very broad peaks. Below 200 kHz the loss data were noisy.

The structural analysis revealed that in HT, one disordered $HCOO^-$ showed flip motion between two *anti*−*syn* orientations. This mainly contributed to the large dielectric responses in HT.[31] On cooling, this motion slowed, leading to the lowering ε' and tanδ, and the minima in tanδ are corresponding to the cases that such flip motion could follow the driving ac field at the respective frequencies and temperatures. Since this flip motion is limited in the c direction, the resulting dipole fluctuation responds more easily to $E\|c$. This is more relevant to the ε_c' and tanδ_c, with higher values and quicker fall on cooling, than it is to the ε_p' and tanδ_p values, because the responses of the powder sample are the averaged ones over all directions, including those less effective $E\perp c$ to drive such flip motion. The wider temperature dispersion of the tanδ_p minima seemingly further supports such argument. When the phase transition happened, the flip motion of the disordered $HCOO^-$ froze, and the spontaneous polarization occurred and pointed to the $-b$ direction, or the polarization is perpendicular to c, as previously discussed. Clearly, these two changes are unfavorable for the dielectric responses to $E\|c$, and thus ε_c' went further down. Instead, the ε_p' included the contribution from the response to $E\perp c$ or $E\|b$, or ε_b' along the polarization direction. As usually observed in ferroelectrics, the ε_b' should increase first when the temperature of the material approaches T_C, and then it should fall below T_C due to the dielectric saturation by the spontaneous polarization.[32] These are what we observed; that is, ε_p' first went to a minimum, then increased to a peak, and finally dropped. In the LT region, the low, slowly changed tanδ responses mainly resulted from the vibration motions of the constituent atoms, with larger values for higher frequencies, inverse to the tanδ responses versus frequency in HT, mainly due to the flip motion of the disordered formato bridges. The significant thermal hysteresis behavior in ε' versus T of **1** indicated the slow kinetic aspect of the phase transition, as DSC data revealed, probably resulting from the large number of defects produced in the transition, as the crystal finely cracked on cooling.[6a,33] For the powder capacitor the thermal hysteresis is much more significant, and the dielectric anomalies shift to lower temperature somewhat, because more defects were produced during the sample preparation, as well as the phase transition.

CONCLUSION

In summary, a new uranyl AMFF of formula $[(C_2H_5)_4N][U_2O_4(HCOO)_5]$ was prepared and characterized. The compound consists of anionic uranyl−formate wavy sheets intercalated by $(C_2H_5)_4N^+$ cations. In the uranyl−formate sheet the pentagonal bipyramidal uranyl cations are connected by equatorial *anti*−*anti* and *anti*−*syn* $HCOO^-$ bridges. The *anti*−*syn* $HCOO^-$ in the nonpolar tetragonal HT phase displays 2-fold disorder, with a flip motion between two *anti*−*syn* orientations. This flip motion slowed on cooling and finally froze, leading to a phase transition at ∼200 K. The LT structure is monoclinic and polar, showing the concerted and net shifts of the ammonium cations along the $-b$ direction with respect to the anionic uranyl−formate sheet; thus, the spontaneous polarization, estimated as 0.86 μC cm^{-2}, occurs in LT. The phase transition is thus HT PE to LT FE, accompanied by significant, anisotropic dielectric anomalies, with quite large thermal hysteresis, and the structure-dielectric property relationship is established. VT luminescent spectroscopy, DSC, and VT crystal photos confirmed the transition and afforded further information. This work demonstrated that the uranyl AMFFs will be of interest for the study of DE/FE/AFE materials and phase transition, and further studies are in progress.

ASSOCIATED CONTENT

Supporting Information

Tabulated data indicating IR and Raman bands and their assignments, illustrations of crystallographic axes, PXRD patterns, and combined TGA and DSC traces; CIF files of crystallography data for the structures in this work. This material is available free of charge via the Internet at http://pubs.acs.org.

AUTHOR INFORMATION

Corresponding Authors

*E-mail: liucl@pku.edu.cn. (C.L.)
*E-mail: zmw@pku.edu.cn. (Z.W.)
*E-mail: gaosong@pku.edu.cn. Fax: 86-10-62751708. (S.G.)

Notes

The authors declare no competing financial interest.

ACKNOWLEDGMENTS

This work was supported by the NSFC (Grants 21171010, 21290171, 11075006, 91026010), the Ministry of Education of the People's Republic of China (Grant 20120001110082), and the State Administration of Science Technology and Industry for National Defense (Grant No. 2012-851).

REFERENCES

(1) (a) Zhou, H.-C.; Long, J. R.; Yaghi, O. M. Eds.; thematic issue on metal-organic frameworks, *Chem. Rev.* **2012**, *112*, 673−674. (b) Long, J. R.; Yaghi, O. M. Eds.; special issue on metal-organic frameworks, *Chem. Soc. Rev.* **2009**, *38*, 1213−1214. (c) Janiak, C.; Vieth, J. K. *New J. Chem.* **2010**, *34*, 2366−2388. (d) Kepert, C. J. *Chem. Commun.* **2006**, 695−700. (e) Cheetham, A. K.; Rao, C. N. R. *Science* **2007**, *318*, 58−59.

(2) (a) Furukawa, H.; Cordova, K. E.; O'Keeffe, M.; Yaghi, O. M. *Science* **2013**, *341*, 1230444−1−1230444−12. (b) Meek, S. T.; Greathouse, J. A.; Allendorf, M. D. *Adv. Mater.* **2011**, *23*, 249−267. (c) Farrusseng, D.; Aguado, S.; Pinel, C. *Angew. Chem., Int. Ed.* **2009**, *48*, 7502−7513. (d) Wei, Y.-S.; Chen, K.-J.; Liao, P.-Q.; Zhu, B.-Y.; Lin, R.-B.; Zhou, H.-L.; Wang, B.-Y.; Xue, W.; Zhang, J.-P.; Chen, X.-M. *Chem. Sci.* **2013**, *4*, 1539−1546. (e) Cairns, A. B.; Goodwin, A. L. *Chem. Soc. Rev.* **2013**, *42*, 4881−4893. (f) Hhorike, S.; Shimomura, S.; Kitagawa, S. *Nat. Chem.* **2009**, *1*, 695−704. (g) Férey, G. *Chem. Soc. Rev.* **2008**, *37*, 191−214. (h) Kitagawa, S.; Kitaura, R.; Noro, S. *Angew. Chem., Int. Ed.* **2004**, *43*, 2334−2375. (i) Morris, R. E.; Bu, X. *Nat. Chem.* **2010**, *2*, 353−361.

(3) (a) Collings, I. E.; Cairns, A. B.; Thompson, A. L.; Parker, J. E.; Tang, C. C.; Tucker, M. G.; Catafesta, J.; Levelut, C.; Haines, J.; Dmitriev, V.; Pattison, P.; Goodwin, A. L. *J. Am. Chem. Soc.* **2013**, *135*, 7610−7620. (b) Spencer, E. C.; Angel, R. J.; Ross, N. L.; Hanson, B. E.; Howard, J. A. K. *J. Am. Chem. Soc.* **2009**, *131*, 4022−4026. (c) Bennett, T. D.; Tan, J. C.; Moggach, S. A.; Galvelis, R.; Mellot-Draznieks, C.; Reisner, B. A.; Thirumurugan, A.; Allan, D. R.; Cheetham, A. K. *Chem.—Eur. J.* **2010**, *16*, 10684−10690. (d) Moggach, S. A.; Bennett, T. D.; Cheetham, A. K. *Angew. Chem., Int. Ed.* **2009**, *48*, 7087−7089.

(4) (a) Zhang, W.; Xiong, R.-G. *Chem. Rev.* **2012**, *112*, 1163−1195. (b) Zhang, W.; Ye, H.-Y.; Xiong, R.-G. *Coord. Chem. Rev.* **2009**, *253*, 2980−2997. (c) Pardo, E.; Train, C.; Liu, H.; Chamoreau, L.-M.; Dkhil, B.; Boubekeur, K.; Lloret, F.; Nakatani, K.; Tokoro, H.; Ohkoshi, S.-i.; Verdaguer, M. *Angew. Chem., Int. Ed.* **2012**, *51*, 8356−8360. (d) Zhang, W.; Cai, Y.; Xiong, R.-G.; Yoshikawa, H.; Awaga, K. *Angew. Chem., Int. Ed.* **2010**, *49*, 6608−6610. (e) Ohkoshi, S.-i.; Tokoro, H.; Matsuda, T.; Takahashi, H.; Irie, H.; Hashimoto, K. *Angew. Chem., Int. Ed.* **2007**, *46*, 3238−3241. (g) Cui, H. B.; Wang, Z. M.; Takahashi, K.; Okano, Y.; Kobayashi, H.; Kobayashi, A. *J. Am. Chem. Soc.* **2006**, *128*, 15074−15075.

(5) (a) Wang, Z. M.; Hu, K. L.; Gao, S.; Kobayashi, H. *Adv. Mater.* **2010**, *22*, 1526−1533. (b) Wang, X.-Y.; Wang, Z.-M.; Gao, S. *Chem. Commun.* **2008**, 281−294. (c) Shang, R.; Chen, S.; Wang, Z. M.; Gao, S. In *Metal-Organic Framework Materials;* Macgillivray, L. R., Lukehart, C. M., Eds.; John Wiley & Sons, Ltd.: Weinheim, Germany, 2014, in press.

(6) (a) Shang, R.; Xu, G. C.; Wang, Z. M.; Gao, S. *Chem.—Eur. J.* **2014**, *20*, 1146−1158. (b) Chen, S.; Shang, R.; Hu, K. L.; Wang, Z. M.; Gao, S. *Inorg. Chem. Front.* **2014**, *1*, 83−98.

(7) (a) Xu, G.-C.; Ma, X.-M.; Zhang, L.; Wang, Z.-M.; Gao, S. *J. Am. Chem. Soc.* **2010**, *132*, 9588−9590. (b) Xu, G.-C.; Zhang, W.; Ma, X.-M.; Chen, Y.-H.; Zhang, L.; Cai, H.-L.; Wang, Z.-M.; Xiong, R.-G.; Gao, S. *J. Am. Chem. Soc.* **2011**, *133*, 14948−14951. (c) Wang, Z. M.; Zhang, B.; Inoue, K.; Fujiwara, H.; Otsuka, T.; Kobayashi, H.; Kurmoo, M. *Inorg. Chem.* **2007**, *46*, 437−445. (d) Li, W.; Probert, M. R.; Kosa, M.; Bennett, T. D.; Thirumurugan, A.; Burwood, R. P.; Parinello, M.; Howard, J. A. K.; Cheetham, A. K. *J. Am. Chem. Soc.* **2012**, *134*, 11940−11943.

(8) (a) Wang, Z. M.; Zhang, B.; Otsuka, T.; Inoue, K.; Kobayashi, H.; Kurmoo, M. *Dalton Trans.* **2004**, 2209−2216. (b) Hu, K.-L.; Kurmoo, M.; Wang, Z.-M.; Gao, S. *Chem.—Eur. J.* **2009**, *15*, 12050−12064. (c) Pato-Doldán, B.; Gómez-Aguirre, L. C.; Bermúdez-García, J. M.; Sánchez-Andújar, M.; Fondado, A.; Mira, J.; Castro-García, S.; Señarís-Rodríguez, M. A. *RSC Adv.* **2013**, *3*, 22404−22411.

(9) (a) Fu, D.-W.; Zhang, W.; Cai, H.-L.; Zhang, Y.; Ge, J.-Z.; Xiong, R.-G.; Huang, S. D.; Nakamura, T. *Angew. Chem., Int. Ed.* **2011**, *50*, 11947−11951. (b) Jain, P.; Ramachandran, V.; Clark, R. J.; Zhou, H. D.; Toby, B. H.; Dalal, N. S.; Kroto, H. W.; Cheetham, A. K. *J. Am. Chem. Soc.* **2009**, *131*, 13625−13627. (c) Jain, P.; Dalal, N. S.; Toby, B. H.; Kroto, H. W.; Cheetham, A. K. *J. Am. Chem. Soc.* **2008**, *130*, 10450−10451. (d) Sánchez-Andújar, M.; Presedo, S.; Yáñez-Vilar, S.; Castro-García, S.; Shamir, J.; Señarís-Rodríguez, M. A. *Inorg. Chem.* **2010**, *49*, 1510−1516. (e) Wang, X. Y.; Gan, L.; Zhang, S. W.; Gao, S. *Inorg. Chem.* **2004**, *43*, 4615−4625.

(10) (a) Zhou, B.; Imai, Y.; Kobayashi, A.; Wang, Z.-M.; Kobayashi, H. *Angew. Chem., Int. Ed.* **2010**, *50*, 11441−11445. (b) Imai, Y.; Zhou, B.; Ito, Y.; Kobayashi, A.; Wang, Z.-M.; Kobayashi, H. *Chem.—Asian J.* **2012**, *7*, 2786−2790.

(11) (a) Hagen, K. S.; Naik, S. G.; Huynh, B. H.; Masello, A.; Christou, G. *J. Am. Chem. Soc.* **2009**, *131*, 7516−7517. (b) Zhao, J.-P.; Hu, B.-W.; Lloret, F.; Tao, J.; Yang, Q.; Zhang, X.-F.; Bu, X.-H. *Inorg. Chem.* **2010**, *49*, 10390−10399. (c) Cañadillas-Delgado, L.; Fabelo, O.; Rodríguez-Velamazán, J. A.; Lemée-Cailleau, M.; Mason, S. A.; Pardo, E.; Lloret, F.; Zhao, J.; Bu, X.; Simonet, V.; Colin, C. V.; Rodríguez-Carvajal, J. *J. Am. Chem. Soc.* **2012**, *134*, 19772−19781.

(12) (a) Li, M.; Liu, B.; Wang, B.; Wang, Z.; Gao, S.; Kurmoo, M. *Dalton Trans.* **2011**, *40*, 6038−6046. (b) Spencer, E. C.; Kiran, M. S. R. N.; Li, W.; Ramamurty, U.; Ross, N. L.; Cheetham, A. K. *Angew. Chem., Int. Ed.* **2014**, *53*, 5583−5586.

(13) (a) Li, M.-Y.; Kurmoo, M.; Wang, Z. M.; Gao, S. *Chem.—Asian J.* **2011**, *6*, 3084−3096. (b) Wang, Z. M.; Zhang, X. Y.; Batten, S. R.; Kurmoo, M.; Gao, S. *Inorg. Chem.* **2007**, *46*, 8439−8441.

(14) Liu, B.; Zheng, H.-B; Wang, Z.-M.; Gao, S. *CrystEngComm* **2011**, *13*, 5285−5288.

(15) (a) Andrews, M. B.; Cahill, C. L. *Chem. Rev.* **2013**, *113*, 1121−1136. (b) Wang, K. X.; Chen, J. S. *Acc. Chem. Res.* **2011**, *44*, 531−540. (c) Giesting, P. A.; Burns, P. C. *Crystallogr. Rev.* **2006**, *12*, 205−255. (d) Gagnon, K. J.; Perry, H. P.; Clearfield, A. *Chem. Rev.* **2012**, *112*, 1034−1054. (e) Loiseau, T.; Mihalcea, I.; Henry, N.; Volkringer, C. *Coor. Chem. Rev.* **2014**, *266−267*, 69−109.

(16) (a) Mentzen, B. F.; Puaux, J. P.; Sautereau, H. *Acta Cryst. B* **1978**, *34*, 1846−1849. (b) Seisenbaeva, G. A.; Polyakov, A. V.; Santalova, N. A.; Dunaeva, K. M. *Koord. Khim.* **1989**, *15*, 1708−1713. (c) Thuery, P. *Inorg. Chem. Commun.* **2008**, *11*, 616−620.

(17) *CrysAlisPro;* Agilent Technologies U.K. Ltd.: Oxford, U.K., 2012.

(18) Sheldrick, G. M. *SHELX-97, Program for Crystal Structure Determination;* University of Göttingen: Göttingen, Germany, 1997.

(19) Zhu, Q. Q.; Wang, L. H.; Liu, C. L.; Wang, Z. M. The 14th International Conference on the Chemistry and Migration Behaviour of Actinides and Fission Products in the Geosphere, Brighton, U.K., September 8−13, 2013; Royal Society of Chemistry: London, U.K., 2013.

(20) White, M. A. In *Crystal Engineering: The Design and Application of Functional Solids;* Seddon, K. R., Zaworotko, M., Eds.; Kluwer Academic Publishers: Dordrecht, Germany, 1999; p 279.

(21) Loopstra, B. O. *J. Inorg. Nucl. Chem.* **1977**, *39*, 1713−1714.

(22) (a) Mentzen, B. F. *Acta Cryst. B* **1977**, *33*, 2546−2549. (b) Mentzen, B. F.; Puaux, J. P.; Sautereau, H. *Acta Cryst. B* **1978**, *34*, 2707−2711. (c) le Roux, S. D.; Van Tets, A.; Adrian, H. W. W. *Acta Crystallogr., Sect B* **1979**, *35*, 3056−3057.

(23) Aizu, K. *Phys. Rev.* **1966**, *146*, 423−429.

(24) (a) Desiraju, G. R.; Steiner, T. *The Weak Hydrogen Bond in Structural Chemistry and Biology;* Oxford University Press: New York, 1999. (b) Steiner, T. *Angew. Chem., Int. Ed.* **2002**, *41*, 48−76.

(25) (a) Williams, D. H.; Fleming, I. *Spectroscopic Method in Organic Chemistry,* 5th ed.; McGraw-Hill Book Co.: Beijing, China, 1998. (b) Nakamoto, K. *Infrared and Raman Spectra of Inorganic and Coordination Compounds;* Wiley: New York, 1986. (c) Stoilova, D.; Koleva, V. *J. Mol. Struct.* **2000**, *553*, 131−139. (d) Stoilova, D.; Koleva, V. *J. Mol. Struct.* **2001**, *560*, 15−21.

(26) (a) Kakihana, M.; Nagumo, T.; Okamoto, M.; Kakihana, H. *J. Phys. Chem.* **1987**, *91*, 6128−6136. (b) Claudel, B.; Mentzen, B.; Navarro, A.; Sautereau, H. *J. Inorg. Nucl. Chem.* **1976**, *38*, 759−762. (c) Lucks, C.; Rossberg, A.; Tsushima, S.; Foerstendorf, H.; Fahmy, K.; Bernhard, G. *Dalton Trans.* **2013**, *42*, 13584−13589.

(27) Bartlett, J. R.; Cooney, R. P. *J. Mol. Struct.* **1989**, *193*, 295−300.

(28) (a) Grohol, D.; Clearfield, A. *J. Am. Chem. Soc.* **1997**, *119*, 4662−4668. (b) Denning, R. G. *J. Phys. Chem. A* **2007**, *111*, 4125−4123. (c) Rabinowitch, E.; Bedford, R. L. *Spectroscopy and Photochemistry of Uranyl Compounds;* Pergamon Press: Oxford, U.K., 1964. (d) Liu, G.; Beitz, J. V. In *The Chemistry of the Actinide and Transactinide Elements;* Morss, L. R., Edelstein, N. M., Fuger, J., Eds.; Springer: Heidelberg, Germany, 2006.

(29) (a) Adelani, P. O.; Oliver, A. G.; Albrecht-Schmitt, T. E. *Cryst. Growth Des.* **2011**, *11*, 3072−3080. (b) Adelani, P. O.; Oliver, A. G.; Albrecht-Schmitt, T. E. *Cryst. Growth Des.* **2011**, *11*, 1966−1973.

(30) Blasse, G.; Grabmaier, B. C. *Luminescent Materials;* Springer-Verlag: Berlin, Germany, 1994.

(31) (a) Jonscher, A. K. *Dielectric Relaxation in Solids;* Chelsea Dielectrics Press: London, U.K., 1983. (b) Yin, Z. W. *Physics of Dielectrics (in Chinese),* 2nd ed.; Science Press: Beijing, China, 2003.

(32) (a) Jona, F.; Shirane, G. *Ferroelectric Crystals;* Pergamon Press: Oxford, U.K., 1962. (b) Känzig, W. *Ferroelectrics and Antiferroelectrics;* Academic Press: New York, 1957.

(33) Lines, M. E.; Glass, A. M. *Principles and Applications of Ferroelectrics and Related Materials;* A Clarendon Press: Oxford, U.K., 1977.